Proceedings (CD) of the 3rd International Conference on Porous Media and its Applications in Science and Engineering
ICPM3
June 20-25, 2010, Montecatini, Italy

VORTEX INSTABILITY OF FREE CONVECTION BOUNDARY LAYERS IN POROUS MEDIA

E. Dodgson[1], D.A.S. Rees[1], R. Scheichl[2]
[1]*Department of Mechanical Engineering, University of Bath, Bath BA2 7AY, UK.*
[2]*Department of Mathematical Sciences, University of Bath, Bath BA2 7AY, UK.*

ABSTRACT

We consider the vortex instability of an inclined free convection boundary layer which is formed adjacent to an impermeable heated surface that is embedded in a porous medium. Many authors have adopted boundary layer theory as the framework within which the stability of this flow is considered. Neutral curves have been obtained showing how the critical distance from the leading edge varies with the wavenumber of the vortex disturbance.

However it is now well-known that such critical distances are too close to the leading edge for the boundary layer approximation to be either valid or accurate. The only exception is when the heated surface is almost vertical but upward-facing. In that case even nonlinear vortices may be studied, but otherwise it is essential that the fully elliptic governing equations are solved, and this latter case forms the topic of the present paper.

On assuming the validity of Darcy's law and the Boussinesq approximation, the momentum equations are written in velocity potential form, and the resulting system, which includes the heat transport equation, is transformed into parabolic coordinates in order to mimic the shape of the spatially-developing boundary layer. These equations are solved using a combination of finite difference approximations and a spanwise Fourier expansion.

It is found that the vortex instability is not an absolute instability because growing disturbances travel downstream faster than they diffuse upstream. However, a steady vortex system may be generated by adopting a suitable boundary condition which induces such a pattern. Our computational results are compared with a parabolic simulation which is valid in the near-vertical limit, and the comparison is excellent.

INTRODUCTION

The topic of boundary layer flows in porous media continues to expand at a prolific rate, although only a very small fraction of published papers are concerned with the stability of those boundary layers. The majority of the papers which deal with instability adopt the classical method, namely that the parallel flow approximation in some form is valid; see, for example, the early paper by Hsu and Cheng [1]. Thus an ordinary differential eigenvalue problem has to be solved to find the critical distance beyond which disturbances grow. Whilst this method will typically give excellent qualitative results, the quantitative data that are produced are often poor.

In this regard, Storesletten and Rees [2] showed that the basic state is insufficiently accurately represented using the boundary layer approximation for consistent stability criteria to be determined. Further, a detailed analysis of the disturbance equations in Rees [3] shows that they cannot be written in a mathematically consistent form whilst insisting that the boundary layer approximation applies. These papers leave open only two possibilities for consistent analysis: (i) the examination of the case where the heated surface is upward facing but almost vertical, and (ii) detailed numerical simulations using the fully elliptic equations. Examples of the first type are the papers by Rees which study, in turn, linear instabilities with respect to streamwise vortices [4], nonlinear vortex evolution [5] and both vortex destabilisation and the effect of isolated disturbances [6]. The present paper is the first to consider the second type of analysis.

In the linear stability analysis of Rees [4], it was shown that a mathematically consistent application of the boundary layer approximation could be applied in the near-vertical limit because the critical

distance for the onset of convection recedes to infinity in that limit. While the basic state, which was first determined by Cheng and Minkowycz [7], is self similar, the fully nonlinear vortex disturbance equations form a parabolic system. Instabilities were initiated by placing a vortex disturbance relatively close to the leading edge and by determining its evolution downstream. A neutral stability curve was obtained by finding where the magnitude of the disturbance begins to grow or begins to decay. Once the vortex enters the nonlinear regime it was found that various strongly nonlinear effects exist, such as saturation and premature decay [5]. This decay is surprising because a local Darcy-Rayleigh number based on the boundary layer thickness continues to increase with distance from the leading edge, and therefore it might be thought that the boundary layer becomes increasingly susceptible to instability. The resolution of this seeming paradox lies in the fact that the evolving vortex pattern becomes subject to subharmonic destabilisation [6]. Thus the wavelength of the pattern increases suddenly to match the increasing boundary layer thickness.

In the present paper we consider vortex instabilities at general inclinations. Figure 1 shows a sketch of the flow domain which we consider.

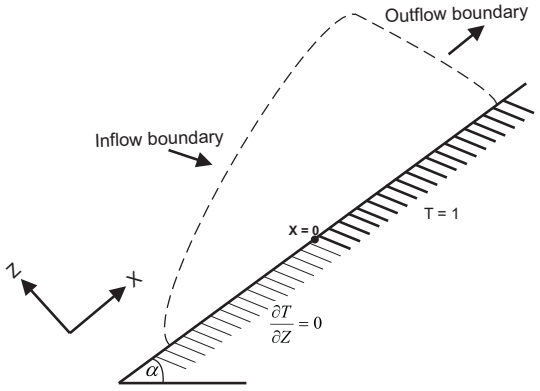

Figure 1. Sketch of the flow domain

Unsteady three-dimensional simulations have been performed in order to compute vortex patterns within such boundary layers. Our preliminary results seem to indicate that the instability is advective in nature, as opposed to being absolute. This means that the upstream diffusion of the vortex pattern is too weak to counter the strength of the basic boundary layer, and disturbances are simply advected away whilst evolving. This is a property which it shares with wave instabilities of the vertical free convection boundary layer of a clear fluid which has been studied by Paul et al. [8]. Therefore we have sought to compare our work with a linear stability theory similar to that of Rees [4] by having vortices initiated by means of a suitable boundary condition. This results in a persistent vortex pattern which can also enter the nonlinear regime.

NOMENCLATURE

A_1, A_2	=	dummy dependent variables
C	=	convergence criterion
g	=	gravitational constant
k	=	wavenumber
K	=	permeability
L	=	natural length scale
N	=	number of Fourier modes
P	=	pressure
q_1	=	surface heat transfer of the vortex
Ra	=	Darcy-Rayleigh number
t	=	time
T	=	temperature
u	=	streamwise velocity
v	=	spanwise velocity
w	=	cross-stream velocity
x	=	streamwise Cartesian coordinate
y	=	spanwise Cartesian coordinate
z	=	cross-stream Cartesian coordinate

Greek symbols

α	=	inclination angle
β	=	expansion coefficient
κ	=	thermal diffusivity
ρ	=	fluid density
θ	=	nondimensional temperature
ϕ	=	velocity potential
μ	=	dynamic viscosity
ξ, η	=	parabolic coordinates
ζ_1, ζ_2	=	dummy coordinates

Subscripts and superscripts

n	=	mode number
$1, 2, 3$	=	velocity potential

GOVERNING EQUATIONS

Darcy's law and the Boussinesq approximation have been assumed. The governing equations in nondimensional form are as follows;

$$\frac{\partial u}{\partial x} + \frac{\partial v}{\partial y} + \frac{\partial w}{\partial z} = 0, \tag{1}$$

$$u = \theta \sin\alpha, \tag{2}$$

$$v = 0, \tag{3}$$

$$w = \theta \cos\alpha, \tag{4}$$

$$\nabla^2\theta = u\frac{\partial\theta}{\partial x} + v\frac{\partial\theta}{\partial y} + w\frac{\partial\theta}{\partial z} + \frac{\partial\theta}{\partial t}. \tag{5}$$

It should be noticed that there is no Darcy-Rayleigh number in these equations. This is because there is no physical lengthscale upon which to base the nondimensionalisation, and therefore we have used

the natural lengthscale,

$$L = \frac{\mu\kappa}{\rho g \beta K \Delta T}, \tag{6}$$

which then yields a unit Darcy-Rayleigh number. A velocity potential,

$$(u, v, w) = \nabla \times (\phi^{(1)}, \phi^{(2)}, \phi^{(3)}), \tag{7}$$

subject to the uniqueness condition that

$$\nabla.(\phi^{(1)}, \phi^{(2)}, \phi^{(3)}) = 0, \tag{8}$$

is introduced; see Aziz and Hellums [9]. The governing equations become

$$\nabla^2\phi^{(1)} = -\frac{\partial\theta}{\partial y}\cos\alpha, \tag{9}$$

$$\nabla^2\phi^{(2)} = \left[\frac{\partial\theta}{\partial x}\cos\alpha - \frac{\partial\theta}{\partial z}\sin\alpha\right], \tag{10}$$

$$\nabla^2\phi^{(3)} = \frac{\partial\theta}{\partial y}\sin\alpha, \tag{11}$$

with the heat transport equation taking the following form

$$\frac{\partial\theta}{\partial t} = \nabla^2\theta + \frac{\partial(\phi^{(1)},\theta)}{\partial(y,z)} + \frac{\partial(\phi^{(2)},\theta)}{\partial(z,x)} + \frac{\partial(\phi^{(3)},\theta)}{\partial(x,y)}, \tag{12}$$

where the Jacobian operator is defined as follows,

$$\frac{\partial(A_1,A_2)}{\partial(\zeta_1,\zeta_2)} = \frac{\partial A_1}{\partial\zeta_1}\frac{\partial A_2}{\partial\zeta_2} - \frac{\partial A_1}{\partial\zeta_2}\frac{\partial A_2}{\partial\zeta_1}. \tag{13}$$

Based upon the exact solution for the vertical boundary layer which was found by Rees and Bassom [10], a parabolic coordinate transformation is introduced. The shape of the resulting mesh mimics the shape of the spatially developing boundary layer and it means that isotherms tend to follow lines of constant values of η. We use

$$x = \frac{1}{4}(\xi^2 - \eta^2), \qquad z = \frac{1}{2}\xi\eta, \tag{14}$$

which is also a Schwarz-Christoffel mapping, and therefore mesh lines are everywhere orthogonal. The heated surface is now at $\eta = 0$ while the insulated part of the bounding surface is at $\xi = 0$. Spanwise Fourier decomposition is then used to reduce the computational effort required to solve the nonlinear equations for the 3D domain. The following Fourier series are introduced;

$$\phi^{(1)} = \sum_{n=1}^{N}\phi_n^{(1)}\sin(nky), \tag{15}$$

$$\phi^{(2)} = \tfrac{1}{2}\phi_0^{(2)} + \sum_{n=1}^{N}\phi_n^{(2)}\cos(nky), \tag{16}$$

$$\phi^{(3)} = \sum_{n=1}^{N}\phi_n^{(3)}\sin(nky), \tag{17}$$

$$\theta = \tfrac{1}{2}\theta_0 + \sum_{n=1}^{N}\theta_n\cos(nky), \tag{18}$$

where θ, $\phi^{(1)}$, $\phi^{(2)}$ and $\phi^{(3)}$ are functions of ξ, η and t. The momentum equations now take the following form:

$$\mathcal{L}_n\phi_n^{(1)} = \frac{(\xi^2+\eta^2)}{4}n\,k\,\theta_n\cos\alpha, \tag{19}$$

$$\mathcal{L}_n\phi_n^{(2)} = \frac{1}{2}\left[\left(\xi\frac{\partial\theta_n}{\partial\xi} - \eta\frac{\partial\theta_n}{\partial\eta}\right)\cos\alpha - \left(\eta\frac{\partial\theta_n}{\partial\xi} + \xi\frac{\partial\theta_n}{\partial\eta}\right)\sin\alpha\right], \tag{20}$$

$$\mathcal{L}_n\phi_n^{(3)} = -\frac{(\xi^2+\eta^2)}{4}n\,k\,\theta_n\sin\alpha, \tag{21}$$

where the elliptic operator, $\mathcal{L}_n$, is defined according to,

$$\mathcal{L}_n\phi = \frac{\partial^2\phi}{\partial\xi^2} + \frac{\partial^2\phi}{\partial\eta^2} - \frac{(\xi^2+\eta^2)}{4}n^2k^2\phi. \tag{22}$$

In the above we have $1 < n < N$ for Eqs. (19) and (21) and $0 < n < N$ for Eq. (20). Substitution into Eq. (12) gives the following

$$\frac{\partial\theta_0}{\partial t} = \frac{4}{(\xi^2+\eta^2)}\left[\mathcal{L}_0\theta_0 + \frac{1}{2}\frac{\partial(\phi_0^{(2)},\theta_0)}{\partial(\eta,\xi)} + 2N_0.\right] \tag{23}$$

where N_0 are the nonlinear terms contributing to the zero mode. For all other modes

$$\begin{aligned}\frac{\partial\theta_n}{\partial t} = \frac{4}{(\xi^2+\eta^2)}\Big[&\mathcal{L}_n\theta_n + N_n \\ &+ \tfrac{1}{4}n\,k\,\phi_n^{(1)}\left(\eta\frac{\partial\theta_0}{\partial\xi} + \xi\frac{\partial\theta_0}{\partial\eta}\right) \\ &+ \tfrac{1}{4}n\,k\,\phi_n^{(3)}\left(-\xi\frac{\partial\theta_0}{\partial\xi} + \eta\frac{\partial\theta_0}{\partial\eta}\right) \\ &+ \tfrac{1}{2}\left(\frac{\partial(\phi_0^{(2)},\theta_n)}{\partial(\eta,\xi)} + \frac{\partial(\phi_n^{(2)},\theta_0)}{\partial(\eta,\xi)}\right)\Big],\end{aligned} \tag{24}$$

where N_n represents the nonlinear terms contributing to mode n. The nonlinear terms arise from the interactions of the modes with each other, modes l

and m give rise to the following terms in mode $(l+m)$ and mode $(l-m)$:

$$\begin{aligned} N_{l\pm m} &= \tfrac{1}{2}\frac{\partial(\phi_l^{(2)},\theta_m)}{\partial(\eta,\xi)} + \frac{lk\phi_l^{(1)}}{4}\left(\eta\frac{\partial\theta_m}{\partial\xi}+\xi\frac{\partial\theta_m}{\partial\eta}\right) \\ &\quad \mp \frac{mk\theta_m}{4}\left(\eta\frac{\partial\phi_l^{(1)}}{\partial\xi}+\xi\frac{\partial\phi_l^{(1)}}{\partial\eta}\right) \\ &\quad \pm \frac{mk\theta_m}{4}\left(\xi\frac{\partial\phi_l^{(3)}}{\partial\xi}-\eta\frac{\partial\phi_l^{(3)}}{\partial\eta}\right) \\ &\quad - \frac{lk\phi_l^{(3)}}{4}\left(\xi\frac{\partial\theta_m}{\partial\xi}-\eta\frac{\partial\theta_m}{\partial\eta}\right). \end{aligned} \tag{25}$$

The following boundary conditions are used;

$$\begin{aligned} \eta = 0: &\ \theta_0 = 2, \quad \theta_1 = 0.01, \\ &\ \phi^{(1)} = \phi^{(2)} = \frac{\partial\phi^{(3)}}{\partial\eta} = 0, \\ \eta = \eta_{\max}: &\ \theta = \phi^{(1)} = \phi^{(3)} = \frac{\partial\phi_0^{(2)}}{\partial\eta} = \phi_n^{(2)} = 0, \\ \xi = 0: &\ \frac{\partial\theta}{\partial\xi} = \phi^{(1)} = \phi^{(2)} = \frac{\partial\phi^{(3)}}{\partial\xi} = 0, \\ \xi = \xi_{\max}: &\ \frac{\partial^2\theta}{\partial\xi^2} = \frac{\partial^2\phi^{(1)}}{\partial\xi^2} = \frac{\partial^2\phi^{(2)}}{\partial\xi^2} = \frac{\partial^2\phi^{(3)}}{\partial\xi^2} = 0. \end{aligned} \tag{26}$$

The values of θ_0 and θ_1 at $\eta = 0$ represent the hot surface and the small-amplitude vortex disturbance, respectively. The boundary conditions at outflow, namely $\xi = \xi_{\max}$, were adopted to give the flow as much freedom to evolve as possible. Other boundary layer simulations have to adopt a buffer region approach in order to maintain numerical stability (see [8], for example), but this did not prove to be necessary here.

NUMERICAL METHOD

The governing equations are discretised spatially using second order accurate central difference approximations and temporally using the first order accurate backwards Euler scheme. The resulting non-linear, implicit equations for all the variables are solved using the multigrid Full Approximation Scheme (FAS). The basic smoother was line Gauss-Seidel in both coordinate directions. We used a 192×64 grid in $0 \le \xi \le 100$ and $0 \le \eta \le 8$. Although our numerical code runs for an arbitrary number, N of modes, the results we present use $N = 1$ as this is sufficient to model the early stages of nonlinearity with self-interaction of mode 1, termed the primary vortex, feeding back into the mean state, mode 0. Variable timestepping is used, reaching a maximum allowable timestep of 3.0. Steady state is deemed to have been reached once

$$\max_{i,j}|\theta_{i,j}^{\text{new}} - \theta_{i,j}^{\text{old}}| < 10^{-8} \tag{27}$$

has been achieved.

RESULTS AND DISCUSSION

The original aim of the present paper was the computation of steady nonlinear vortex patterns with thermal boundary layers of various inclinations from the horizontal. The near-vertical linear analysis of Rees [4] suggests that useful guideline values of the critical distance and wavenumber for such vortices are,

$$\xi = 17.940\frac{\sqrt{\sin\alpha}}{\cos\alpha}, \qquad k = 0.05723\cos\alpha, \tag{28}$$

Therefore, for an inclination of say, 55°, one ought to have $\xi = 28.31$ and $k = 0.0328$. When we used a computational domain which extends as far as $\xi = 100$, and for a variety of wavenumbers centred on the above value, small-amplitude vortex disturbances, once introduced, were found to grow whilst advecting downstream. However, in all cases it was found that the disturbances leave the computational domain via the outflow boundary and leave behind what is the steady two-dimensional basic state. Therefore a tentative hypothesis is that the instability is advective in nature, rather than absolute. Although the review of Rees [3] shows that approximate methods of analysing vortex instability yield inconsistent results, it is clear that the advective nature of the instability demonstrates that what appears in practice is very different from what is suggested by all neutral stability criteria that have been published to date.

We have therefore turned our attention to the generation of vortices using temperature modulations on the heated surface; see the condition for θ_1 in Eq. (26). The linearised stability theory developed by Rees [4] involved the placing of a disturbance within a near-vertical boundary layer and the monitoring of its evolution downstream using a parabolic solver. The code used there has been modified for the present paper to one where the vortex mode is forced by means of an identical nonzero boundary condition for the primary vortex mode. When ξ is sufficiently small, the temperature gradient at the surface is negative, but thermoconvective instability soon causes the amplitude of the vortex to grow. Therefore the temperature gradient eventually changes sign to reflect the fact that the temperature in the bulk is higher than the surface temperature.

(a)

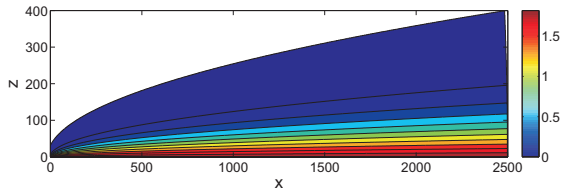

(b)

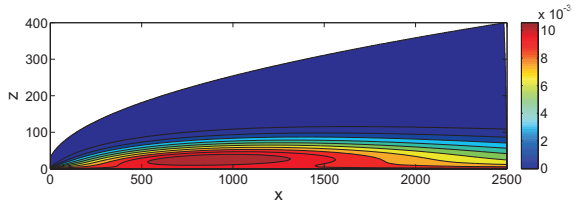

Figure 2. Isotherms for (a) θ_0, (b) θ_1, for $k = 0.06$ and $\alpha = 55°$.

(a)

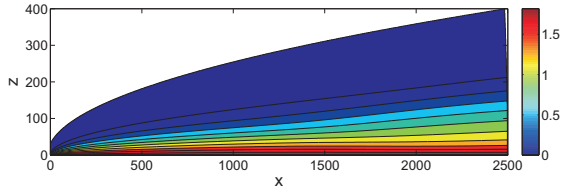

(b)

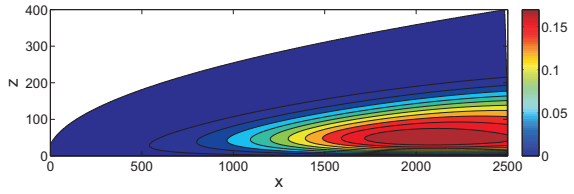

Figure 3. Isotherms for (a) θ_0, (b) θ_1, for $k = 0.04$ and $\alpha = 55°$.

(a)

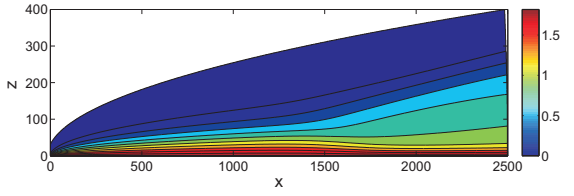

(b)

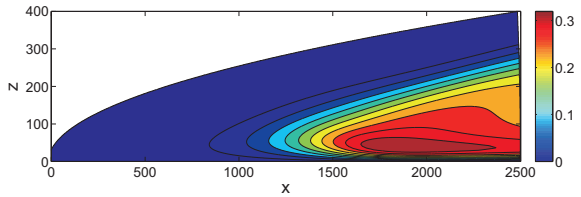

Figure 4. Isotherms for (a) θ_0, (b) θ_1, for $k = 0.025$ and $\alpha = 55°$.

We define ξ_0 to be that position at which the temperature gradient changes sign and although this will clearly be downstream of the neutral location this value affords a simple means by which the parabolic simulations may be compared with the present elliptic ones. When translated into the present notation, our parabolic simulations yield the following value of ξ_0 and and the wavenumber, k_0, which minimises ξ_0:

$$\xi_0 = 23.49\frac{\sqrt{\sin\alpha}}{\cos\alpha}, \qquad k_0 = 0.0703\cos\alpha. \tag{29}$$

Figures 2 to 4 show isotherms for the mean temperature field, θ_0, and the primary vortex, θ_1 for an inclination of 55° from the horizontal, and for the wavenumbers, $k = 0.06$, 0.04 and 0.025, respectively. The basic temperature field for this inclination is represented very well by Fig. 2a, because the vortex has remained weak.

Figure 2 corresponds to $k = 0.06$, a value which is above the value given in Eq. (29) when $\alpha = 55°$. Such values of k have only finite ranges of ξ within which growth may occur according to the neutral curve. This Figure demonstrates this clearly and the maximum value of θ_1 arises at $x \simeq 850$. However, the strength of the vortex pattern is not large, and the θ_0 isotherms are graphically indistinguishable from the basic state.

The corresponding situation for $k = 0.04$ is shown in Figure 3. Here we see a vortex pattern which has enjoyed a longer region of growth, although it reaches a maximum at $x \simeq 2100$. By comparing Figs. 2a and 3a we see that there is a slight change in the isotherm pattern for θ_0; clearly convection has become moderately nonlinear.

When $k = 0.025$, Figure 4 shows a vortex profile which is stronger than those for the larger wavenumbers, although it begins its growth at a larger value of x (or ξ) than when $k = 0.04$. The strength of the growth of the vortex has modified the mean temperature profile, θ_0, quite substantially, and it is quite clear that the mean rate of heat transfer at the surface has been enhanced substantially in this case.

Having reviewed the steady pattern obtained for three different wavenumbers, it is also interesting to note how the thickness of the vortex system (in terms of η) varies with wavenumber. It is clear that the vortex becomes increasingly confined towards the heated surface as k increases. This fact is related to the presence of the $-n^2k^2$ coefficient in the definition of the operator, $\mathcal{L}_n$, in Eq. (22), which generates an exponentially decaying solution that is proportional to $\exp(-nk\eta)$.

Further computations were undertaken for other values of k. In all these cases the surface rate of heat transfer, $q_1 = \partial\theta_1/\partial\eta|_{\eta=0}$, for the primary vortex

was recorded as a function of ξ, and are shown in Fig. 5. The growth phase for each wavenumber is seen clearly, as is the beginning of the decay phase, although the curve for $k = 0.1$ always decays.

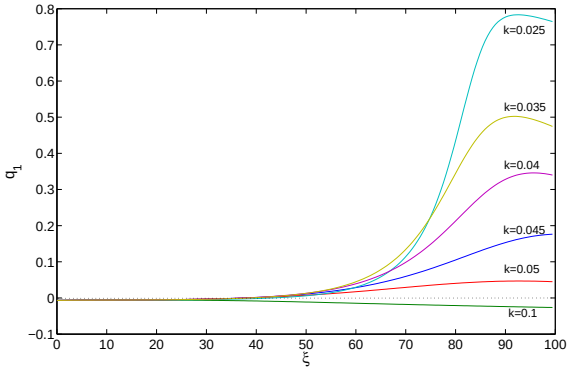

Figure 5. Variation of q_1 with ξ for a variety of wavenumbers.

For the sake of comparison with the associated parabolic simulation, the dependence of ξ_0 (for which $q_1 = 0$) on the wavenumber is given in the Table:

k	ξ_0
0.025	43.00
0.035	38.28
0.040	37.24
0.045	37.25
0.050	38.30
0.060	51.82

Table 1. Dependence of ξ_0 on k.

On fitting a parabola through the smallest value of ξ_0 and its two nearest neighbours we obtain the following values for the minimum:

$$\xi_0 = 37.11, \qquad k_0 = 0.0425. \tag{30}$$

When we substitute $\alpha = 55^\circ$ into Eqs. (29), the following values have been found:

$$\xi_0 = 37.07, \qquad k_0 = 0.0403, \tag{31}$$

which compares very well indeed. We would certainly expect an even closer match as the angle of inclination increases, although wave-like convection has been found to occur at smaller inclinations.

CONCLUSIONS

In this short paper we have undertaken unsteady three-dimensional simulations of streamwise vortices in a free convection boundary layer in porous media. Contrary to expectation, we have found that vortex instabilities are advective in nature at moderate angles of inclination. Upon forcing a stationary vortex structure by means of thermally modulated boundary conditions we have found a very strong correlation between the present elliptic computations and the parabolic system which pertains when the heated surface is almost vertical.

REFERENCES

[1] C. T. Hsu and P. Cheng, "Vortex instability in buoyancy-induced flow over inclined heated surfaces in porous media," *Trans. A.S.M.E. J. Heat Transf.*, vol. 101, pp. 660–665, 1979.

[2] L. Storesletten and D. A. S. Rees, "The influence of higher-order effects on the linear instability of thermal boundary layer flow in porous media," *Int. J. Heat Mass Transf.*, vol. 41, pp. 1833–1843, 1998.

[3] D. A. S. Rees, "Thermal boundary-layer instabilities in porous media: A critical review," in *Transport Phenomena in Porous Media* (D. B. Ingham and I. Pop, eds.), Pergamon, 1998.

[4] D. A. S. Rees, "Vortex instability from a near-vertical heated surface in a porous medium I. Linear instability," *Proc. R. Soc. Lond. A*, vol. 457, pp. 1721–1734, 2001.

[5] D. A. S. Rees, "Vortex instability from a near-vertical heated surface in a porous medium II. Nonlinear evolution," *Proc. R. Soc. Lond. A*, vol. 458, pp. 1575–1592, 2002.

[6] D. A. S. Rees, "Nonlinear vortex development in free convective boundary layers in porous media," in *NATO ASI Proceedings*, (Neptun, Romania), pp. 449–458, June 2003.

[7] P. Cheng and W. J. Minkowycz, "Free convection about a vertical flat plate embedded in a porous medium with application to heat transfer from a dike," *J. Geophys. Res.*, vol. 82, pp. 2040–2044, 1977.

[8] M. C. Paul, D. A. S. Rees, and M. Wilson, "Receptivity of free convective flow from a heated vertical surface. i. linear waves," *Int. J. Thermal Sciences*, vol. 47, pp. 1382–1392, 2008.

[9] K. Aziz and J. D. Hellums, "Numerical solution of the three-dimensional equations of motion for laminar natural convection," *Phys. Fluids*, vol. 10, pp. 314–324, 1967.

[10] D. A. S. Rees and A. P. Bassom, "Some exact solutions for free convective flows over heated semi-infinite surfaces in porous media," *Int. J. Heat Mass Transf.*, vol. 34, pp. 1564–1567, 1991.